Why charging Li-air batteries with current low-voltage mediators is slow and singlet oxygen does not explain degradation

Sunyhik Ahn[1], Ceren Zor[1], Sixie Yang[1], Marco Lagnoni[2], Daniel Dewar[1], Tammy Nimmo[1], Chloe Chau[1], Max Jenkins[1], Alexander J. Kibler[3], Alexander Pateman[1], Gregory J. Rees[1], Xiangwen Gao[1], Paul Adamson[1], Nicole Grobert[1], Antonio Bertei[2], Lee R. Johnson[3], and Peter G. Bruce[1,4]*

[1]*Department of Materials, University of Oxford, Oxford, U.K.*

[2]*Department of Civil and Industrial Engineering, University of Pisa, Pisa, Italy*

[3]*Nottingham Applied Materials and Interfaces Group, School of Chemistry, University of Nottingham, Nottingham, U.K.*

[4]*Department of Chemistry, University of Oxford, Oxford, U.K.*

Abstract

While Li–air rechargeable batteries offer higher energy densities than lithium-ion batteries, the insulating Li_2O_2 formed during discharge hinders rapid, efficient re-charging. Redox mediators are used to facilitate Li_2O_2 oxidation, however, fast kinetics at low charging voltage is necessary for practical applications but has yet to be achieved. We investigate the mechanism of Li_2O_2 oxidation by redox mediators. The rate-limiting step is the outer sphere 1 e^- oxidation of Li_2O_2 to LiO_2, which follows Marcus theory. The second step is dominated by LiO_2 disproportionation, forming mostly triplet O_2. The yield of singlet O_2 depends on the redox potential of the mediator in a way that does not correlate with electrolyte degradation, in contrast to earlier views. Our mechanistic understanding explains why current low-voltage mediators (< +3.3 V) fail to deliver high rates (the maximum rate is at +3.74 V) and suggests important mediator design strategies to deliver sufficiently high rates for fast charging at potentials closer to the thermodynamic potential of Li_2O_2 oxidation (+2.96 V).

Li-O_2 batteries have the potential to offer a step-change in specific energy over Li-ion battery chemistries.[1–4] The reaction at the cathode involves the reduction of O_2 to Li_2O_2 on discharge and its

oxidation back to O_2 on charge. However, the insulating nature of Li_2O_2 renders these electrochemical reactions slow and inefficient.[5] In particular, on charging, the electrochemical oxidation of Li_2O_2 leads to potentials 1-1.5 V higher than the thermodynamic potential of +2.96 V vs. Li^+/Li, with the consequence of poor round trip energy efficiency.[6] Strategies that have been explored to circumvent this issue include use of heterogeneous solid state catalysts,[7,8] and use of soluble redox mediators (RM).[9–12] The benefit of using soluble redox mediators is their ability to oxidise Li_2O_2 particles within the porous cathode that are not in direct contact with the electrode surface. RMs are oxidised at the cathode surface, diffuse to the Li_2O_2 particles, then oxidise Li_2O_2 liberating O_2 and reforming the reduced RM, such that the cycle then repeats.[13–19] RMs with redox potentials up to +3.9 V have been reported and those with high potentials enable high charging rates but lead to very poor round trip energy efficiency, while those close to the thermodynamic potential of +2.96 V are too slow to support even moderate charging rates. Mediators operating close to the thermodynamic potential and with fast kinetics are required. Furthermore, it has been suggested that oxidation of Li_2O_2 leads to singlet oxygen ($^1O_2$) as well as the ground triplet state ($^3O_2$).[20,21] This area of research remains a topic of debate.[22] $^1O_2$ is known to be a reactive species and has been implicated in the degradation of the electrolyte and carbon cathode. There is evidence that $^1O_2$ can be suppressed by charging at low voltage.[23] Despite several interesting studies into charging RMs,[16,24–28] questions regarding the process of Li_2O_2 oxidation by RMs remain. A recent report by Petit et al. examined the oxidation of alkali peroxides by redox mediators, including their mechanism and the relation of mediator potential with $^1O_2$ formation.[28] However, the reported results do not seem to accord with the known trends in rate performance versus voltage and O_2 evolution discussed above.[25,29] Resolving this complex mechanism is essential if a RM operating close to the thermodynamic potential of +2.96 V vs. Li^+/Li with sufficient kinetics to sustain fast charging and the ability to suppress $^1O_2$ is ever to be realised.

Here we report the mechanism of Li_2O_2 oxidation by RMs and its influence on $^1O_2$ evolution. We show, by analysing $^1O_2$ and $^3O_2$ evolution, that the rate determining step for Li_2O_2 oxidation is the initial outer sphere 1 e^- oxidation of Li_2O_2 to form LiO_2 ($RM^+ + Li_2O_2 \leftrightarrows RM + LiO_2 + Li^+$). It follows Marcus theory with a maximum rate at +3.74 V. We show that current low voltage mediators provide lower oxidation rates compared to current higher voltage mediators, consistent with known charging behaviour of Li-O_2 cells. We show that the dominant subsequent step is the disproportionation of LiO_2 to $^3O_2$ ($2LiO_2 \leftrightarrows Li_2O_2 + {}^3O_2$) and not the 1 e^- oxidation of LiO_2 to $^1O_2$ or $^3O_2$, ($RM^+ + LiO_2 \leftrightarrows RM + {}^3O_2 + Li^+$ and $RM^+ + LiO_2 \leftrightarrows RM + {}^1O_2 + Li^+$). We also show how mediators with different potentials affect the $^1O_2$ yield and that this does not correlate well with degradation, casting doubt on whether $^1O_2$ is the major source of degradation during charge. Our mechanism not only explains why the current generation of mediators cannot deliver high charging rates at sufficiently low potentials for good round trip energy efficiency, but also points the way to designing mediators that could deliver high rates at low charge voltages.

Results and discussion

Marcus theory explains redox mediator kinetics

To investigate the mechanism of oxidation of Li_2O_2 by RMs, eq. 1, the charging process in a Li-O_2 battery, the rate constants for this reaction using RMs with redox potentials (E_{RM}) that span from +3.2 V to +3.9 *V* vs. Li^+/Li were measured, Fig. 1A.

$$2RM^+ + Li_2O_2 \leftrightarrows 2RM + O_2 + 2Li^+ \qquad \text{(eq. 1)}$$

While it would be desirable to measure rate constants for the elementary steps, the intermediate LiO_2 cannot be isolated and kinetic measurements for oxidation of other alkali superoxides are highly dependent on the counter ion and electrolyte environment, Fig. S2, making such an analysis of questionable use.[30,31] Consequently, we obtain an effective rate constant for the overall reaction which will be dominated by the rate determining step. Scanning electrochemical microscopy (SECM) is a widely utilised tool for quantification of heterogeneous electron transfer rate constants.[32–34] This method accurately models mass transport effects, which if not taken into account can mask true kinetic constants.[35] We also highlight that some mediators are prone to decomposition with the electrolyte, which can lower the effective concentration and thus the efficacy of kinetic measurements. For example, Fig. S3 shows that amount of oxygen evolved during Li_2O_2 oxidation by aged $TEMPO^+$ solutions decrease significantly with age, consistent with side reactions between $TEMPO^+$ and the electrolyte solution. During the SECM measurement, reactive intermediates are only formed transiently and thus the method is free from such errors. SECM has been applied previously to study Li_2O_2.[27,36] Here, SECM was employed using the set-up illustrated in Fig. 1A to measure the effective rate constant (k_{eff}) for the reaction of RM^+ with Li_2O_2. This is achieved by performing approach curves where an ultramicroelectrode (UME) is lowered towards a disk of Li_2O_2. The RM is oxidised to RM^+ at the UME, then reacts with the Li_2O_2 disk generating a feedback loop and

a modulation of the current as a function of distance. The rate of reaction in eq. 1 can be determined by subsequent fitting of the feedback approach curves using the methodology developed by Cornut.[27,37,38] The resulting feedback approach curves for a selection of RMs are shown in Figure 1B, where a higher current at low UME-Li_2O_2 distances indicates a higher k_{eff}. k_{eff} is proportional to the rate constant of the rate determining step in the sequence of steps during mediated Li_2O_2 oxidation (eq. 2a-e). The k_{eff} values for TMPD and DMPZ were too low to be measured by SECM and so were measured using a pressure cell method, where Li_2O_2 and RM^+ are mixed together in a gas tight cell and the pressure change from O_2 evolution is measured as a function of time. Formation of the Li_2O_2 disk, construction of the SECM cell, determination of the E_{RM} from cyclic voltammetry, pressure cell methodology, data treatment and additional supporting data are described in the methods and Fig. S4, S5 and S6.

$$RM^+ + Li_2O_2 \leftrightarrows RM + LiO_2 + Li^+ \qquad \text{(eq. 2a)}$$

$$RM^+ + LiO_2 \leftrightarrows RM + {}^3O_2 + Li^+ \quad \text{(eq. 2b)}$$

$$RM^+ + LiO_2 \leftrightarrows RM + {}^1O_2 + Li^+ \quad \text{(eq. 2c)}$$

$$2LiO_2 \leftrightarrows Li_2O_2 + {}^3O_2 \quad \text{(eq. 2d)}$$

$$2LiO_2 \leftrightarrows Li_2O_2 + {}^1O_2 \quad \text{(eq. 2e)}$$

Plotting ln k_{eff} of RMs as a function of E_{RM}, results in the volcano shaped plot shown in Fig. 1C. The values for TTF and TEMPO are in accord with previous studies.[36] The shape of the curve in Fig. 1C suggests Marcus theory for an electron transfer rate constant (k_{et}) as expressed in eq. 3;[39]

$$k_{et} = Z_{el} exp\left[\frac{-[(\lambda - F(E_{RM} - E_{Li_2O_2}))]^2}{4\lambda RT}\right] \quad \text{(eq. 3)}$$

where k_{eff} is proportional to k_{et}, $E_{Li_2O_2}$ is the redox potential of Li_2O_2, Z_{el} is the pre-exponential constant, and λ is the reorganisation energy. The variation of λ across different RMs is estimated to be small due to their similar molecular volumes and any contribution from the Li_2O_2 is constant (see SI). Fitting eq. 3 to the data in Fig. 1C shows agreement between the variation of k_{eff} with E_{RM} and the trend predicted by Marcus theory, including the observation of an inverted region. This implies that the rate determining step is a single outer-sphere electron transfer process. The fitted values are: E_{Li2O2} = +3.41 V, λ = 0.322 eV and Z_{el} = 0.00495. Marcus theory, originally devised for electron transfer between molecules, has been applied previously to electron transfer between wide band gap solids and redox molecules, including ZnO and PtO.[34,40,41] Li_2O_2 is a wide band gap solid composed of discrete O_2^{2-} molecules coordinated by Li^+.[5,42] The reorganisation energy (λ), can be modified by changing the electrolyte environment. λ is greater for glyme solvents containing TBA^+ salts compared to alkali metal salts due to differences in dielectric constants.[43] Plotting the ln k_{eff} as a function of E_{RM}, for various electrolyte compositions (E_{RM} measured for each electrolyte composition as described in the SI), where Li^+ is increasingly replaced by TBA^+, results in the Marcus volcano plots shifting to the right as the concentration of TBA^+ increases (Fig. 2). According to Marcus theory (eq. 3), the apex of the volcano (the highest rate of oxidation) occurs when $F\Delta E = \lambda$, hence with increasing λ, the volcano shifts to more positive E_{RM}. The broadening of the volcanoes is also consistent with an increase in λ.[39] These results further demonstrate that the kinetics of Li_2O_2 oxidation by RMs can be explained by an outer-sphere one electron transfer from Li_2O_2 to the RM^+. Our trend of rate vs. RM^+ potential is in accord with the known behaviour of Li-O_2 cells with mediators.[25,29,36] We compare our results with kinetic studies by Ko et al. and Petit et al., and also with the trend of O_2 evolution from mediated cells by Kwak et al., Fig. S6A.To further validate our observed trend, we used pressure monitoring, as described in the methods section, to measured O_2 evolution during Li_2O_2 oxidation by TEMPO·BF_4 and DMPZ·BF_4, Fig. S6B. The pressure measurements show much more rapid O_2 release with TEMPO than DMPZ, in contrast to the results of Petit et al.

Thermodynamically, Li_2O_2 oxidation is possible for any mediator with a potential > +2.96 V, however, this does not answer the question of what overpotential is required for practical charging rates. Using a model for the porous cathode of a Li-O_2 cell as shown in Fig. 3A and B, and described in more detail in the methods section, together with the k_{eff} and E_{RM} determined for each mediator, galvanostatic

charging profiles were simulated to identify the limits of charging rate for mediated cells, assuming ideal Li^+ transport in the electrolyte and no oxygen bubbling. The simulated galvanostatic charging for selected RMs are shown in Fig. S7. In each case the charging voltage was simulated as a function of the state of charge for different charging current densities and up to a cut off of +4 V. Towards the end of charging, when Li_2O_2 is depleted the total surface area of Li_2O_2 is diminished, the rate of Li_2O_2 oxidation will slow and drive the potential up. This is why the potentials rise rapidly towards the end of charge and that 100% charging is not possible as it would require infinite potential. Higher current densities will result in earlier onset of polarisation, as shown in Fig. S7. In Fig. 3C we show the maximum rate of charge possible for different RMs to achieve 99.75% state of charge. Full details of the simulation can be found in the methods section. The rate of RM oxidation at the electrode surface, $k_{o,het}$, and the mass transport of RM between the surface and the Li_2O_2 particles are fast, thus the rate limiting process is the RM^+ oxidation of Li_2O_2. The results in Fig. 3C demonstrate that the lower voltage RMs can only sustain charging at low rates before polarising to +4 V; the maximum charging rates for DMPZ and TMPD to achieve > 99% charge capacity are ≤ 0.1 mA cm^{-2} (Fig. 3C). Whereas for high voltage mediators such as MAZO or TEMPO, charging at ≥ 40 mA cm^{-2} is possible. We qualitatively verify the results of the model by charging lab-scale Li-O_2 cells connected to an on-line mass spectrometer. Fig. 3F shows that a cell containing TEMPO can be charged and evolved significant oxygen. In contrast, Fig. 3D and E shows that a cell containing DMPZ or TMPD only oxidizes the RM, without detectable release of oxygen. For these latter cells, although direct oxidation of Li_2O_2 at the electrode surface is possible, the electrodes are prepared by drop casting giving poor contact, coupled with the slow mediator kinetics and relatively small amounts of Li_2O_2 in an electrode, O_2 evolution is suppressed below +4 V.[44] These results are consistent with other studies of Li-O_2 cells, which also find that neither DMPZ nor TMPD are able to sustain high charging rates and high coulombic efficiency for O_2.[15,24,45] We cannot replicate the conditions used in the simulation, specifically the current lack of a true gas diffusion electrode for an organic metal-air battery means that O_2 is not transported efficiently through the thick porous electrode, resulting in Li_2O_2 accumulating at the air interphase, blocking the pores. The implication of our simulations and experiments is that to achieve high rates of charge, RMs with undesirably high charging voltages (poor round trip energy efficiency) are required. This highlight why it is important to understand the mechanism of RM^+ oxidation of Li_2O_2 in order to guide the search for new RMs with high kinetics at low voltage.

Singlet oxygen evolution and the reaction mechanism

Oxidation of Li_2O_2 forms first LiO_2 (eq. 2a), the latter then goes on to evolve O_2 in the ground state triplet $^3O_2$ or excited state singlet $^1O_2$ by two pathways, oxidation of LiO_2 (eq. 2b and c) or LiO_2 disproportionation (eq. 2d and e).[22] Overall Li_2O_2 oxidation should lead to a charge to oxygen ratio $e^-/O_2 = 2$, however, it has been reported for both unmediated and mediated charging that this value is often greater than 2, suggesting the occurrence of parasitic side reactions.[46–48] Such parasitic reactions have been attributed to attack of the electrolyte solution and/or carbon cathode by reactive singlet oxygen ($^1O_2$). The charging voltage has been shown to impact $^1O_2$ yield (i.e. the percentage of $^1O_2/(^1O_2 + {}^3O_2)$).[21,23] $^1O_2$ yields from charging a Li-O_2 cell with RMs have been explored prior to this study.[26] We quantify $^1O_2$ yields by mixing Li_2O_2 with chemically oxidised redox mediators (RM^+) in tetraglyme to understand the role of RM^+ oxidation in $^1O_2$ yield. This analysis also allows us to establish which of the steps in eq. 2 are limiting the rate of the overall oxidation of Li_2O_2, the first or second e^- transfer or the disproportionation. The results are presented in Fig. 4. The amount of $^3O_2$ was quantified using online mass spectrometry and $^1O_2$ by capturing it in solution using 9,10-dimethylanthracene (DMA),[21] a selective chemical trap that reacts rapidly with $^1O_2$ to form DMA-endoperoxide, which is then

quantified using HPLC (Fig. 4A). The yield of $^1O_2$ for each mediator is expressed as a percentage of the total O_2 evolved and plotted as a function of E_{RM} in Fig. 4B. We note that our trend differs to that obtained by Petit et al.,[28] thus we further validated the results using an alternative method employing nuclear magnetic resonance (NMR) spectroscopy, which can identify reacted DMA with greater chemical specificity than the UV-Vis method (Fig. S10). Full details of both methods can be found in the methods section. This data confirms the trend shown. To determine the yield of $^1O_2$ that arises directly from the chemical disproportionation of LiO_2 alone, KO_2 was mixed with a tetraglyme solution containing Li^+ and 6-crown ether, which induces spontaneous disproportionation of the former via eq. 2d and 2e.[49,50] This reaction offers the closest surrogate to that occurring in the lithium-air battery and has been used widely in the field, although we note it cannot fully recreate this reaction. The reaction yields 0.23% $^1O_2$, represented by the pink dotted line in Fig. 4B. As seen in Fig. 4B, higher $^1O_2$ yields than occur from disproportionation alone are observed for RMs between 3.2 to 3.5 *V* vs. Li^+/Li whereas for RMs with E_{RM} ≥ 3.6 V a constant, potential-independent yield of $^1O_2$ is observed, consistent with the yield from only chemical disproportionation.

Consideration of the data shown in Fig. 1 and 4 together offers significant insight into the charge mechanism. We know from Fig. 1 that the rate determining step for Li_2O_2 oxidation is either the first or second 1 e^- oxidation, i.e., either Li_2O_2 → LiO_2 or LiO_2 → $^1O_2$ or $^3O_2$. In Fig. 4B, the $^1O_2$ evolved in excess of that from LiO_2 disproportionation must originate from the second e^- transfer i.e. LiO_2 oxidation to form $^1O_2$ (eq. 2c). Comparing the trend for k_{eff} in Fig. 1, the effective rate constant for the rate limiting step during Li_2O_2 oxidation, with the trend for the proportion of $^1O_2$ formed in Fig. 4B, it is clear that the rate limiting step is not $LiO_2 + RM^+$ → $Li^+ + {}^1O_2 + RM$. Since the potential corresponding to the maximum rate of Li_2O_2 oxidation, Fig. 1, is not coincident with the highest proportion of $^1O_2$ in Fig. 4B. In fact, at the maximum k_{eff}, $^1O_2$ is formed by disproportionation alone. Following a similar argument, we can rule out $LiO_2 + RM^+$ → $Li^+ + {}^3O_2 + RM$ as the rate determining step, as again the potential of the highest k_{eff} does not correspond to any increase in the proportion of $^3O_2$ over that obtained from disproportionation alone. The rate limiting step is therefore the first e^- oxidation of Li_2O_2; $RM^+ + Li_2O_2 \leftrightarrows RM + LiO_2 + Li^+$ (eq. 2a). The analysis of the $^1O_2$ yields can also reveal the relative rates of the four second steps in the oxidation of Li_2O_2, i.e., steps represented by eq. 2b to 2e. The yield of $^1O_2$ in Fig. 4B shows that the dominant O_2 product is $^3O_2$ and therefore the dominant 2nd step is one that forms $^3O_2$ not $^1O_2$. Considering the two routes for $^3O_2$ formation, disproportionation and $LiO_2 + RM^+$ → $Li^+ + {}^3O_2 + RM$ (eq. 2b and d), $^3O_2$ is predicted to be 0.97 eV lower in energy than $^1O_2$.[20,51] Fig. 4B show $LiO_2 + RM^+$ → $Li^+ + {}^1O_2 + RM$ occurs at E_{RM} of 3.2 to 3.5 V and the general shape of the curve suggests that mediated LiO_2 oxidation may also follow a Marcus relationship. Based on this assumption, $LiO_2 + RM^+$ → $Li^+ + {}^3O_2 + RM$ is expected to occur < +2.96 V vs. Li^+/Li. This means that $LiO_2 + RM^+$ → $Li^+ + {}^3O_2 + RM$ is already driven far to the right for all potentials at which Li_2O_2 is oxidised. The fact that we do not observe $^3O_2$ proportions greater than that from disproportionation despite the required thermodynamic potential for $LiO_2 + RM^+$ → $Li^+ + {}^3O_2 + RM$, implies that the kinetics of this step is negligible. The reaction, $RM^+ + LiO_2$ → $RM + Li^+ + {}^1O_2$ competes for LiO_2 with disproportionation. With increasing RM potential, the rate of Li_2O_2 oxidation to form LiO_2 increases, increasing the LiO_2 concentration and decreasing the RM^+ concentration, thus favouring LiO_2 disproportionation. In short, the amount of LiO_2 and RM^+ available for $RM^+ + LiO_2$ → $RM + Li^+ + {}^1O_2$ is not a constant, skewing somewhat the peak shown in Fig. 4.

In summary, we can conclude that the rate limiting step for Li_2O_2 oxidation is the outer sphere 1 e^- oxidation of Li_2O_2 to LiO_2, eq. 2a. Also, that the dominant 2nd step is $^3O_2$ evolution by LiO_2

disproportionation. The overall mechanism is shown in the schematic in Fig. 5. The values for the reorganisation energy, λ, along with E_{Li2O2}/E_{LiO2} and Z_{el} are presented in Table S2 where they are compared with those from Petit et al. In line with the different trends in rate constant with RM potential between the present study and that of Petit et al, all the values are different.

Implications for the Li-O_2 battery

The fundamental understanding of the Li_2O_2 oxidation mechanism presented here explains why within the current generation of mediators those that operate at a low potential and therefore good round trip energy efficiently, < +3.3 V, do not deliver sufficiently high charging rates. The mechanistic understanding also shows how new mediators might be designed to give high rates at low potentials, which is essential if Li-air batteries are to be realised. The optimal redox mediator is one that charges at a low potential, just sufficient to drive the reaction thermodynamically, i.e., approx. +3 *V vs. Li^+/Li*, that does so with fast kinetics and with the minimum of reactive $^1O_2$ formed. However, as is clear in Fig. 1, the highest rate is obtained at E_{RM} of ca. +3.7 V, which does not fit the first requirement for a high rate at a low charging voltage. Given that the rate limiting step follows Marcus kinetics it is possible to show how fast kinetics at a low voltage might be achieved. Considering the Marcus equation (eq. 3), for a low voltage RM close to $E_{Li_2O_2}$, a low activation energy and hence fast kinetics of Li_2O_2 oxidation, k_{eff} is obtained by minimising the reorganisation energy λ.[39,52–54] This directs future synthesis to RMs that undergo minimal structural change between oxidation states and to electrolytes with low dielectric constants. The former requires the reduced and oxidised forms of the mediator to have very similar sizes and molecular geometry, e.g. as found in some large delocalised electron molecules. Our computational modelling shows that RMs with intermediate redox potentials of +3.4 V can achieve charging rates of 1 mA cm^{-2}. Hence a relatively small reduction in λ may allow practical charging rates to be achieved at low voltage, closer to +3 V.

However, while searching for such mediators is desirable it may not be sufficient. λ also contains a contribution from the Li_2O_2 surface and while different facets of the Li_2O_2 crystal may exhibit different λ they are intrinsic to the material. The analysis here implies that it may be necessary to seek redox mediators that operate by an inner sphere mechanism, to achieve higher rates than can be obtained solely by minimizing the reorganizational energy of the mediator. In other words, adsorb onto the surface, interacting with it and opening the possibility of circumventing the limitations of outer sphere and hence Marcus behaviour. Furthermore, the analysis described here shows that formation of reactive $^1O_2$ reaches a maximum for RMs with E_{RM} of approx. +3.45 V, but drops near to the baseline value of $^1O_2$ formation, (i.e via disproportionation), when below +3.2 V. Therefore, a RM with the desirable low voltage will also minimise the amount of $^1O_2$ formation. It is interesting to note that for RMs operating at potentials which generate the maximum amount of $^1O_2$, approx. +3.45 *V*, the e^-/O_2 ratio is close to 2 (TTF, +3.39 V, e^-/O_2 = 2.03-2.06)[15] and very similar to the e^-/O_2 for mediators operating at potentials where the $^1O_2$ yield is low, e.g. TEMPO (+3.77 V, e^-/O_2 = 2.05)[55] In addition, it is well known that degradation and side reactions during charging of a Li-O_2 cell occur most significantly above 3.6 V when $^1O_2$ release is lowest.[23,46,56] These results imply that $^1O_2$ may not be the major source of parasitic side reactions on charging, and the role of superoxide and CO_2 which are known to cause capacity fade, should not be underestimated.[57,58]

Acknowledgements

Wenjun Xu, Dr. Yujia Qing and Prof. Hagan Bayley from the Department of Chemistry, University of Oxford are gratefully acknowledged for access and technical assistance with HPLC. L.R.J. thanks the University of Nottingham's Propulsion Futures Beacon for funding towards this research and acknowledges financial support from the EPSRC (EP/S001611/1) and the Faraday Institution (EP/S003053/1 FIRG014). P.G.B. acknowledges financial support from the EPSRC (EP/M009521/1) and the Henry Royce Institute for Advanced Materials (EP/R00661X/1, EP/S019367/1, EP/R010145/1).

Author Contributions Statement

S.A., D.D, and T. N. performed SECM and pressure cell measurements and analysed the data. S.A., C.Z., A.P, and S.Y., performed online mass spectrometry and HPLC experiments. A.K., S.A., C.Z., C.C, M.J., and D.D synthesized, purified and characterised redox mediators. S.Y. and T. N. constructed Li-O_2 cells coupled to online-MS and analysed the data. S.Y., C.C., and X.G. performed UV-Vis measurements. M.L. and A.B. wrote and implemented computational code for simulations. G.J.R., C.Z., and D.D performed online mass spectrometry and NMR measurements. P.G.B, L.R.J., S.A., X.G., C.Z, G.J.R. and P.A analysed and interpreted the data. P.G.B. wrote the manuscript with contributions from L.R.J., A.B. and S.A. P.A., N.G., L.R.J., and P.G.B supervised the project.

Competing Interests Statement

The authors declare no competing interests

Figure Legends/Captions

Figure 1. Kinetic analysis showing that RM mediated oxidation of Li_2O_2 follows Marcus kinetics. A) Schematic representation of ultramicrodisk electrode (UME) used for the scanning electrochemical microscopy (SECM) set-up with molecular structures and redox potentials (E_{RM}) of the RM. B) SECM approach curves to Li_2O_2 for selected redox mediators plotted on dimensionless axes (as per standard practice in SECM analysis, line: experimental data, dots: model fitting).[27,37] Data for other RMs can be found in Fig. S1 in the Supplementary Information. C) Marcus plot of ln k_{eff} as a function of E_{RM} in 0.1 M LiTFSI in tetraglyme. Error bars represent 1 standard deviation from an average of three measurements. The dotted line is the fit to the data by the Marcus equation using the least-squares method ($E_{Li2O2} = +3.41$ V, $\lambda = 0.322$ eV and $Z_{el} = 0.00495$, $R^2 = 0.98$)

Figure 2. Li^+ concentration affects kinetics of Li_2O_2 oxidation consistent with Marcus theory. Plot of ln k_{eff} (RM^+ reaction with Li_2O_2) as a function of E_{RM}, for varying ratios of TBA^+:Li^+ while total concentration $TFSI^-$ in tetraglyme is kept constant. Error bars show 1 standard deviation from an average of three measurements. The dotted line is the fit to the data by the Marcus equation using the least-squares method.

Figure 3. Simulations of lithium-O_2 cell charging, showing that low voltage RMs cannot sustain moderate charging rates. A) Schematic representation of the porous cathode model used to calculate galvanostatic charging of a lithium-air battery with RMs; porous carbon gas diffusion electrode 100 μm thick with 40% of the

internal electrode volume filled with 400 nm diameter Li_2O_2 particles at the beginning of charge. B) The particle size decreases as oxidation proceeds. C) Maximum charging rate ($I_{max.}$) that reaches 99.75% state of charge as a function of RM's E_{RM} according to the cathode model in Fig. 3A. Further details of the simulations can be found in the SI and the data is tabulated in Table S1. D), E) & F) Experimental galvanostatic charging profiles of Li-O_2 cathodes pre-loaded with Li_2O_2, electrolyte 1 M LiTFSI in tetraglyme with 10 mM DMPZ (D), 10 mM TMPD (E), and 10 mM TEMPO (F) coupled to on-line mass spectrometry for detection of evolved oxygen. Cells were charged at 0.065 mA cm^{-2}. Galvanostatic charging at a higher current of 0.3 mA cm^{-2} is reported in Fig. S8 and shows the same behaviour. The black dotted line presents O_2 flux expected from oxidation of Li_2O_2 to O_2 ($2e^-/O_2$). Data on additional mass fragments can be found in Fig. S9.

Figure 4. Relationship between RM redox voltage and singlet oxygen yield. A) Singlet oxygen yields (percentage of $^1O_2/(^1O_2 + ^3O_2)$) from different RMs as a function of their redox potential (E_{RM}) and comparison with that from LiO_2 disproportionation (dotted line). Error bars represent 1 standard deviation from an average of three measurements. See Table S1 for tabulated values. B) Example of online mass spectrometry of gaseous products ($^3O_2$ in black and CO_2 in red) from sampling headspace of the reaction vessel in the case of $TEMPO^+$ reaction with Li_2O_2. C) HPLC analysis from sampling the liquid solution of from the completed reaction in C). The solution contains DMA, which is added and reacts irreversibly with $^1O_2$ to form DMA-O_2, which is detected by HPLC.

Figure 5. The first e^- transfer step to oxidize Li_2O_2 is the rate determining step. Schematic illustration of the reaction mechanism of RM facilitated Li_2O_2 oxidation. The thicknesses of the arrows correspond to the relative rates of reaction.

References

1. Ma, L. *et al.* Fundamental Understanding and Material Challenges in Rechargeable Nonaqueous Li–O2 Batteries: Recent Progress and Perspective. *Adv. Energy Mater.* **8**, 1800348 (2018).

2. Liu, T. *et al.* Current Challenges and Routes Forward for Nonaqueous Lithium-Air Batteries. *Chemical Reviews* (2020) doi:10.1021/acs.chemrev.9b00545.

3. Kwak, W. J. *et al.* Lithium-Oxygen Batteries and Related Systems: Potential, Status, and Future. *ACS Appl. Mater. Interfaces* **120**, 6626–6683 (2020).

4. Wang, D., Mu, X., He, P. & Zhou, H. Materials for advanced Li-O2 batteries: Explorations, challenges and prospects. *Mater. Today* **26**, 87–99 (2019).

5. Viswanathan, V. *et al.* Electrical conductivity in Li2O2 and its role in determining capacity limitations in non-aqueous Li-O2 batteries. *J. Chem. Phys.* **135**, 214704 (2011).

6. Gallant, B. M. *et al.* Influence of Li2O2 morphology on oxygen reduction and evolution kinetics in Li-O2 batteries. *Energy Environ. Sci.* **6**, 2518–2528 (2013).

7. Li, F. *et al.* Superior Performance of a Li-O2 Battery with Metallic RuO2 Hollow Spheres as the Carbon-Free Cathode. *Adv. Energy Mater.* **5**, 2–7 (2015).

8. Tan, P., Wei, Z. H., Shyy, W., Zhao, T. S. & Zhu, X. B. A nano-structured RuO2/NiO cathode

enables the operation of non-aqueous lithium-air batteries in ambient air. *Energy Environ. Sci.* **9**, 1783–1793 (2016).

9. Park, J.-B., Lee, S. H., Jung, H.-G., Aurbach, D. & Sun, Y.-K. Redox Mediators for Li-O $_2$ Batteries: Status and Perspectives. *Adv. Mater.* **1704162**, 1704162 (2017).

10. McCloskey, B. D. & Addison, D. A Viewpoint on Heterogeneous Electrocatalysis and Redox Mediation in Nonaqueous Li-O2Batteries. *ACS Catal.* **7**, 772–778 (2017).

11. Liu, T. *et al.* The Effect of Water on Quinone Redox Mediators in Nonaqueous Li-O2Batteries. *J. Am. Chem. Soc.* **140**, 1428–1437 (2018).

12. Lacey, M. J., Frith, J. T. & Owen, J. R. A redox shuttle to facilitate oxygen reduction in the lithium air battery. *Electrochem. commun.* **26**, 74–76 (2013).

13. Chase, G.; Zecevic, S.; Walker, W.; Uddin, J.; Sasaki, K.; Giordani, V.; Bryantsev, V.; Blanco, M.; Addison, D. Soluble oxygen evolving catalysts for rechargeable metal-air batteries. *WO Pat.* 2,011,133 (2011).

14. Bergner, B. J., Schürmann, A., Peppler, K., Garsuch, A. & Janek, J. TEMPO: A Mobile Catalyst for Rechargeable Li-O2 Batteries. *J. Am. Chem. Soc.* **136**, 15054–15064 (2014).

15. Chen, Y., Freunberger, S. A., Peng, Z., Fontaine, O. & Bruce, P. G. Charging a Li-O2 battery using a redox mediator. *Nat. Chem.* **5**, 489–494 (2013).

16. Lim, H. D. *et al.* Rational design of redox mediators for advanced Li-O2 batteries. *Nat. Energy* **1**, (2016).

17. Kundu, D., Black, R., Adams, B. & Nazar, L. F. A highly active low voltage redox mediator for enhanced rechargeability of lithium-oxygen batteries. *ACS Cent. Sci.* **1**, 510–515 (2015).

18. Zhang, T., Liao, K., He, P. & Zhou, H. A self-defense redox mediator for efficient lithium-O2 batteries. *Energy Environ. Sci.* **9**, 1024–1030 (2016).

19. Yao, K. P. C. *et al.* Utilization of Cobalt Bis(terpyridine) Metal Complex as Soluble Redox Mediator in Li-O2 Batteries. *J. Phys. Chem. C* **120**, 16290–16297 (2016).

20. Mourad, E. *et al.* Singlet oxygen from cation driven superoxide disproportionation and consequences for aprotic metal-O $_2$ batteries. *Energy Environ. Sci.* **2**, 2559–2568 (2019).

21. Mahne, N. *et al.* Singlet oxygen generation as a major cause for parasitic reactions during cycling of aprotic lithium-oxygen batteries. *Nat. Energy* **2**, 1–9 (2017).

22. Schurmann, A., Luerßen, B., Mollenhauer, D., Janek, J. & Der, D. S. Singlet Oxygen in Electrochemical Cells : A Critical Review of Literature and Theory. *Chem. Rev.* **121**, 12445–12464 (2021).

23. Wandt, J., Jakes, P., Granwehr, J., Gasteiger, H. A. & Eichel, R. A. Singlet Oxygen Formation during the Charging Process of an Aprotic Lithium-Oxygen Battery. *Angew. Chemie - Int. Ed.* **55**, 6892–6895 (2016).

24. Bawol, P. P. *et al.* A new thin layer cell for battery related DEMS-experiments: The activity of redox mediators in the Li-O2 cell. *Phys. Chem. Chem. Phys.* **20**, 21447–21456 (2018).

25. Ko, Y. *et al.* A comparative kinetic study of redox mediators for high-power lithium-oxygen batteries. *J. Mater. Chem. A* **7**, 6491–6498 (2019).

26. Liang, Z., Zou, Q., Xie, J. & Lu, Y.-C. Suppressing singlet oxygen generation in lithium–oxygen batteries with redox mediators. *Energy Environ. Sci.* **13**, 2870–2877 (2020).

27. Chen, Y., Gao, X., Johnson, L. R. & Bruce, P. G. Kinetics of lithium peroxide oxidation by redox mediators and consequences for the lithium-oxygen cell. *Nat. Commun.* **9**, 1–6 (2018).

28. Petit, Y. K. *et al.* Mechanism of mediated alkali peroxide oxidation and triplet versus singlet oxygen formation. *Nat. Chem.* (2021) doi:10.1038/s41557-021-00643-z.

29. Kwak, W. J. *et al.* Oxidation Stability of Organic Redox Mediators as Mobile Catalysts in Lithium-Oxygen Batteries. *ACS Energy Lett.* **5**, 2122–2129 (2020).

30. Laoire, C. O., Mukerjee, S., Abraham, K. M., Plichta, E. J. & Hendrickson, M. A. Influence of nonaqueous solvents on the electrochemistry of oxygen in the rechargeable lithium-air battery. *J. Phys. Chem. C* **114**, 9178–9186 (2010).

31. Bryantsev, V. S., Blanco, M. & Faglioni, F. Stability of lithium superoxide LiO2 in the gas phase: Computational study of dimerization and disproportionation reactions. *J. Phys. Chem. A* **114**, 8165–8169 (2010).

32. Unwin, P. R. & Bard, A. J. Scanning electrochemical microscopy 9. Theory and application of the feedback mode to the measurement of following chemical reaction rates in electrode processes. *J. Phys. Chem.* **95**, 7814–7824 (1991).

33. Arroyo-Currás, N. & Bard, A. J. Iridium oxidation as observed by surface interrogation scanning electrochemical microscopy. *J. Phys. Chem. C* **119**, 8147–8154 (2015).

34. Rodríguez-López, J., Minguzzi, A. & Bard, A. J. Reaction of various reductants with oxide films on Pt electrodes As studied by the surface interrogation mode of scanning electrochemical microscopy (SI-SECM): Possible validity of a Marcus relationship. *J. Phys. Chem. C* **114**, 18645–18655 (2010).

35. Miller, J. R., Beitz, J. V. & Huddleston, R. K. Effect of Free Energy on Rates of Electron Transfer between Molecules. *J. Am. Chem. Soc.* **106**, 5057–5068 (1984).

36. Krueger, B., Rucker, K. K. & Wittstock, G. Redox Mediators for Faster Lithium Peroxide Oxidation in a Lithium–Oxygen Cell: A Scanning Electrochemical Microscopy Study. *ACS Appl. Energy Mater.* **5**, 3724–3733 (2022).

37. Lefrou, C. & Cornut, R. Analytical Expressions for Quantitative Scanning Electrochemical Microscopy (SECM). *ChemPhyscChem* **11**, 547–556 (2010).

38. Cornut, R. & Lefrou, C. New analytical approximation of feedback approach curves with a microdisk SECM tip and irreversible kinetic reaction at the substrate. *J. Electroanal. Chem.* **621**, 178–184 (2008).

39. Marcus, R. A. On the Theory of Electron-Transfer Reactions. VI. Unified Treatment for Homogeneous and Electrode Reactions. *J. Chem. Phys.* **43**, 679–701 (1965).

40. Nakabayashi, S., Itoh, K., Fujishima, A. & Honda, K. Electron transfer rates in highly exothermic reactions on semiconductor-electrolyte interfaces, and the deuterium isotope effect. *J. Phys. Chem.* **87**, 5301–5303 (1983).

41. Hamann, T. W., Gstrein, F., Brunschwig, B. S. & Lewis, N. S. Measurement of the free-energy dependence of interfacial charge-transfer rate constants using ZnO/H2O semiconductor/liquid contacts. *J. Am. Chem. Soc.* **127**, 7815–7824 (2005).

42. Gerbig, O., Merkle, R. & Maier, J. Electron and ion transport in Li2O2. *Adv. Mater.* **25**, 3129–3133 (2013).

43. Barthel, J. & Feuerlein, F. Dielectric properties of propylene carbonate-1,2-dimethoxyethane

mixtures and their electrolyte solutions of NaClO4 and Bu4NClO4. *Zeitschrift fur Phys. Chemie* **148**, 157–170 (1986).

44. Meini, S. *et al.* Rechargeability of Li-air cathodes pre-filled with discharge products using an ether-based electrolyte solution: Implications for cycle-life of Li-air cells. *Phys. Chem. Chem. Phys.* **15**, 11478–11493 (2013).

45. Lim, H. D. *et al.* Rational design of redox mediators for advanced Li-O2batteries. *Nat. Energy* **1**, (2016).

46. Mccloskey, B. D. *et al.* Combining accurate O2 and Li2O2 assays to separate discharge and charge stability limitations in nonaqueous Li-O 2 Batteries. *J. Phys. Chem. Lett.* **4**, 2989–2993 (2013).

47. Schwenke, K. U., Meini, S., Wu, X., Gasteiger, H. A. & Piana, M. Stability of superoxide radicals in glyme solvents for non-aqueous Li-O2 battery electrolytes. *Phys. Chem. Chem. Phys.* **15**, 11830–11839 (2013).

48. Tong, B., Huang, J., Zhou, Z. & Peng, Z. The Salt Matters: Enhanced Reversibility of Li–O 2 Batteries with a Li[(CF 3 SO 2)(n-C 4 F 9 SO 2)N]-Based Electrolyte. *Adv. Mater.* **30**, 1–6 (2018).

49. Black, R. *et al.* Screening for superoxide reactivity in Li-O 2 batteries: Effect on Li 2 O 2 /LiOH crystallization. *J. Am. Chem. Soc.* **134**, 2902–2905 (2012).

50. Peng, Z. *et al.* Oxygen reactions in a non-aqueous Li+ electrolyte. *Angew. Chemie - Int. Ed.* **50**, 6351–6355 (2011).

51. Kwabi, D. G. *et al.* Experimental and Computational Analysis of the Solvent-Dependent O2/Li+-O2- Redox Couple: Standard Potentials, Coupling Strength, and Implications for Lithium-Oxygen Batteries. *Angew. Chemie - Int. Ed.* **55**, 3129–3134 (2016).

52. Ihly, R. *et al.* Tuning the driving force for exciton dissociation in single-walled carbon nanotube heterojunctions. *Nat. Chem.* **8**, 603–609 (2016).

53. Gruhn, N. E. *et al.* The vibrational reorganization energy in pentacene: Molecular influences on charge transport. *J. Am. Chem. Soc.* **124**, 7918–7919 (2002).

54. Farver, O., Marshall, N. M., Wherland, S., Lu, Y. & Pecht, I. Designed azurins show lower reorganization free energies for intraprotein electron transfer. *Proc. Natl. Acad. Sci. U. S. A.* **110**, 10536–10540 (2013).

55. Gao, X., Chen, Y., Johnson, L. R., Jovanov, Z. P. & Bruce, P. G. A rechargeable lithium-oxygen battery with dual mediators stabilizing the carbon cathode. *Nat. Energy* **17118**, 1–7 (2017).

56. Adams, B. D. *et al.* Towards a stable organic electrolyte for the lithium oxygen battery. *Adv. Energy Mater.* **5**, 1–11 (2015).

57. Kwabi, D. G. *et al.* Chemical instability of dimethyl sulfoxide in lithium-air batteries. *J. Phys. Chem. Lett.* **5**, 2850–2856 (2014).

58. Zhang, S. *et al.* On the incompatibility of lithium-O2 battery technology with CO2. *Chem. Sci.* **8**, 6117–6122 (2017).

Methods

Chemicals and Materials

Bis(trifluoromethane)sulfonimide lithium salt (LiTFSI, 99.99%, Sigma Aldrich) was dried under vacuum at 120 °C for 24 hours. Tetrabutylammonium Bis(trifluoromethane)sulfonimidate (TBATFSI, >99% Sigma Aldrich) was dried under vacuum at 70 °C for 48 hours. Tetraethylene glycol dimethyl ether (tetraglyme, > 99%, Sigma Aldrich) was distilled over benzophenone and sodium and left to dry with freshly activated molecular sieves for at least 5 days before use. The water content of all electrolytes was quantified to be below 10 ppm by Karl-Fisher titration. Redox mediators 2,2,6,6-tetramethyl-1-piperidinyloxy (TEMPO, 99%, Sigma-Aldrich), 4-methoxy-2,2,6,6-tetramethyl-1-piperidinyloxy (M-TEMPO, 97%, Sigma-Aldrich) 1-methyl-2-azaadamantane-*N*-oxyl (MAZO, 97%, Sigma-Aldrich), *N*-methylphenothiazine (MPT, 98%, Sigma-Aldrich), 10-isopropylphenothiazine (PPT, 98%, Sigma Aldrich), ferrocene (Fc, 98%, Sigma-Aldrich), tetrathiafulvalene (TTF, 97%, Sigma-Aldrich), *N*,*N*,*N*′,*N*′-tetramethyl-*p*-phenylenediamine (TMPD, 99%, Sigma-Aldrich) and 5,10-dihydro-5,10-dimethylphenazine (DMPZ, 99%, TCI), Phenothiazine (PT, >98%, Merck) and 1,5-dimethyl-9-azanoradamantane N-oxyl (DMN-AZO, 95%, Fujifilm Wako) were used as purchased. 3,7-dibromo-10-ethylphenothiazine (DBrEPT, >99%) was synthesized according to a literature procedure.[59] 5,10,15,20-Tetraphenyl-21H,23H-porphone (TPP, >99%, Sigma-Aldrich) and 9,10-Dimethylanthracene (DMA, Alfa Aesar, 99.9%) were used as purchased. Selected redox mediators were chemically oxidised following established methods.[60–63] The Li_2O_2 was synthesised in-house by following established methods.[64] H_2O_2 (30% wt., 99.999% purity trace metal basis, Sigma Aldrich) was added dropwise to LiOH (99.999%, Sigma Aldrich) solvated in distilled methanol with rapid stirring. The white precipitate was filtered and washed with more distilled methanol and left to dry under vacuum at 70 °C for at least 48 hours. XRD analysis confirmed formation of Li_2O_2 (Fig. S11), and $KMnO_4$ titration estimates > 99% purity compared to 94% for commercially purchased Li_2O_2 (technical grade, Sigma Aldrich). Li_2O_2 powder was pressed into 6 mm diameter disks with a die set at 1 tonne pressure. All synthesis and disk pressing were conducted in a nitrogen glovebox with < 1 ppm H_2O and O_2.

Electrochemical analysis

All electrochemical measurements and electrolyte preparation were conducted in a nitrogen glovebox with < 1 ppm H_2O and O_2. A commercial scanning electrochemical microscopy (SECM) set-up (CH Instruments model 920D, CH Instruments, USA) was used with a 12.5 µm Au microdisk working electrode and fritted partially delithiated $LiFePO_4$ (LFP) counter and reference electrodes (two separate electrodes). The R_g factor of the working electrode was determined by comparing the ratio of steady-state currents at a sharpened electrode to that obtained at an equivalent non-sharpened electrode following the methodology by Cornut.[37] The effective reaction constant (k_{eff}) for the reaction between the RMs and Li_2O_2 was determined by measuring the current as a function of electrode-Li_2O_2 disk distance. The microdisk electrode approach speed was 1.5 µm per second. This approach curve was fit using an analytical model developed by Cornut (eq. 4a-d).[37,38,65] The modelling is carried out using dimensionless variables as is standard in SECM analysis. $\mathrm{I_n}$ is the electrode current divided by the steady state current at large electrode-Li_2O_2 distances, L is the electrode-Li_2O_2 distance divided by the electrode radius (r), and Λ is the dimensionless rate constant for the reaction of Li_2O_2 with RM given by eq. S4d and D is the diffusion coefficient of the RM.

$$I_n = \alpha(R_g) + \frac{\pi}{4\beta(R_g)\mathrm{ArcTan}\left(L+\frac{1}{\Lambda}\right)} + \left(1-\alpha(R_g)-\frac{1}{2\beta(R_g)}\right)\frac{2}{\pi}\mathrm{ArcTan}\left(L+\frac{1}{\Lambda}\right) + \frac{\left(\frac{\frac{2.08}{R_g^{0.358}}\left(L-\frac{0.145}{R_g}\right)+1.585}{\frac{2.08}{R_g^{0.358}}(L+0.0023R_g)+1.57+\frac{\ln R_g}{L}+\frac{2}{\pi R_g}\ln\left(1+\frac{\pi R_g}{2L}\right)}\right)^{-1}}{(1+2.47R_g^{0.31}L\Lambda)(1+L^{0.006R_g+0.113}\Lambda^{-0.0236R_g+0.91})}$$ (eq. 4a)

$$\alpha(R_g) = \ln 2 + \ln 2\left(1-\frac{2}{\pi}\mathrm{ArcCos}\frac{1}{R_g}\right) - \ln 2\left(1-\left(\frac{2}{\pi}\mathrm{ArcCos}\left(\frac{1}{R_g}\right)\right)^2\right)$$ (eq. 4b)

$$\beta(R_g) = 1 + 0.639\left(1-\frac{2}{\pi}\mathrm{ArcCos}\frac{1}{R_g}\right) - 0.186\left(1-\left(\frac{2}{\pi}\mathrm{ArcCos}\left(\frac{1}{R_g}\right)\right)^2\right)$$ (eq. 4c)

$$\Lambda = \frac{rk_{eff}}{D}$$ (eq. 4d)

The diffusion coefficients of redox mediators were calculated from microdisk steady-state chronoamperometry. Redox potentials of the redox mediators (*E_{RM}*) were estimated by fitting microdisc voltammetry data using commercial DigiElch 4F simulation software (Elchsoft, Germany) as shown in Fig. S4, and the resulting values are given in Table S1.

For experiments with varying Li^+ and TBA^+ content in the electrolyte, the total $TFSI^-$ concentration was kept constant at 400 mM, *E_{RM}* were measured in each solvent composition. The average radius of the RM molecules, a, was estimated by calculating the van der Waals volume following the cited procedure and by approximating that RMs have a spherical shape and the resulting values are given in Table S1.[66] The variation in average molecular radii is small, hence λ_{ET} from the Marcus equation, 5, is similar for RMs studied here.[39]

$$\lambda_{ET} = \frac{e_0^2}{4\pi\epsilon_0}\left(\frac{1}{\epsilon_{op}} - \frac{1}{\epsilon_s}\right)\frac{1}{2a} \quad (eq.\,5)$$

The Marcus equation, eq. 3, was fit to the kinetic data using a least-squares method. The fit values for λ is 0.322 eV and Z_{el} is 0.00495, and the correlation between Marcus plot and experiments R^2 is 0.980 (values are tabulated in Table S2). The fit value for E_{Li2O2} = +3.41 V, which is within the range of simulated $E_{Li2O2/LiO2}$ voltage range found in literature.[67] We note that Petit et al. used $E_{Li2O2/O2}$, but this assumes a direct 2-electron transfer from Li_2O_2 to form O_2 whereas oxidation occurs via step-wise single electron transfers due to 2-electron transfer steps having high kinetic barriers.[68]

Oxygen evolution measurements for kinetic analysis

A custom-made stainless-steel pressure cell, illustrated in Fig. S5A was constructed to measure the rate of oxygen evolution when solid Li_2O_2 is mixed with solutions of pre-oxidised redox mediators. This method was used for RMs whose kinetics were too slow to be measured by SECM. The reaction chamber which is sealed from the main body of the cell by a valve, contained a saturated solution of RM^+ and additional solid RM^+ which was added to maintain a saturated RM^+ concentration in solution during reaction with Li_2O_2. Sufficient Li_2O_2 was added into the main body of the pressure cell, to maintain a relatively constant reaction surface area during the reaction. The pressure cell was placed in a temperature-controlled incubator set to 298 K and allowed to equilibrate prior to opening the

valve to mix the RM^+ solution with Li_2O_2 to initiate the reaction. During reaction, the mixture was stirred rapidly using a stirrer bar while the pressure is measured with a pressure transducer (PX409, Omega Engineering). Representative results are shown in Fig. S5C and D. The rate of reaction is proportional to the pressure-time gradient. This gradient is normalised by the concentration of RM^+ in solution and mass of Li_2O_2 and replotted in Fig. S5B. The normalised pressure-time gradient is converted to k_{eff} values using TEMPO as the calibration. The k_{eff} values from pressure measurements are in good accord with the trends from SECM experiments, as shown in Fig. S5E.

Gas diffusion electrode (GDE) electrochemical model

The electrochemical model developed for this work serves as a tool to evaluate the effect on the electrochemical performance of different redox mediators at a cell scale, elucidating intrinsic limitations given by different mediators' kinetics and transport properties determined with experimental measures throughout this work (such as diffusion coefficient and k_{eff} shown in Table S1). The electrochemical model for a gas diffusion electrode (GDE) is illustrated in Fig. 3A in the main text. The cathode is modelled based on parameters for binder-free carbon paper used in a prior study[69] while the anode is considered ideal. The model used to simulate the electrochemical behaviour and mass transport was coded in Comsol Multiphysics software. The general molar balance equation for species *i* (Li^+, $TFSI^-$, RM, RM^+ and e^-) is shown in eq. 6, where c_i is the species molar concentration and ε is the porosity, which increases with time upon Li_2O_2 oxidation. Generalised Poisson-Nernst-Planck (PNP) equations are used to compute species fluxes (N_i), taking into account diffusion, migration and convection due to electrolyte displacement. Galvanostatic charging voltage profiles are simulated by setting a rate of species consumption and/or production along the thickness of the electrode, according to their stoichiometric coefficient ($\nu_{i,j}$), as a consequence of the mediator oxidation reaction (eq. 7a) and Li_2O_2 oxidation (eq. 7b, which is equivalent to eq. 1). The electrode voltage, concentration changes and resulting molecular flux are simulated as follows. The volumetric reaction rate of redox mediator oxidation $\left(\dot{R}^v_{het}\right)$ is represented by Butler-Volmer kinetics (eq. 8), where $k_{o,het}$ is the charge-transfer kinetic constant, s^v_{el} the electrode specific surface area per unit volume, α is the transfer coefficient and η_{act} the activation overpotential, which depends on the electrode and electrolyte potentials (ϕ_{el} and ϕ_{ey}). The volumetric Li_2O_2 oxidation reaction $\left(\dot{R}^v_{eff}\right)$ follows elementary reversible chemical kinetics (eq. 9), where $s^v_{Li_2O_2}$ is the specific surface area of Li_2O_2 particles (which shrink with time), a_{Li^+} is the activity of Li^+ and K^{eq}_{eff} is the equilibrium constant of Li_2O_2 oxidation. Oxygen transport is assumed to be fast such that there is no accumulation of oxygen bubbles: similarly, Li^+ and $TFSI^-$ transport are assumed to be fast to neglect ohmic losses in the electrolyte to emphasize the intrinsic limitations of mediator kinetics. The simulations are run until the voltage limit of +4 V is reached. A range of galvanostatic charging currents are tested to find the maximum current that allows 99.75% conversion of Li_2O_2 into O_2 within this voltage limit.

$$\frac{\partial}{\partial t}(\varepsilon c_i) + \frac{\partial}{\partial x} N_i = \sum_j \nu_{i,j} \dot{R}^v_j \qquad \text{(eq. 6)}$$

$$RM \leftrightarrows RM^+ + e^- \qquad \text{(eq. 7a)}$$

$$\frac{1}{2} Li_2O_2 + RM^+ \leftrightarrows Li^+ + \frac{1}{2} O_2 + RM \qquad \text{(eq. 7b)}$$

$$\dot{R}^v_{het} = s^v_{el} k_{o,het} c_{RM^+}{}^{(1-\alpha)} c_{RM}{}^{\alpha} \left\{ \exp\left((1-\alpha) \frac{F}{RT} \eta_{act} \right) - \exp\left(-\alpha \frac{F}{RT} \eta_{act} \right) \right\} \qquad \text{(eq. 8a)}$$

$$\eta_{act} = \phi_{el}\text{-}\phi_{ey}\text{-}E_{RM} + \frac{RT}{F}\ln\left(\frac{c_{RM}}{c_{RM^+}}\right) \qquad \text{(eq. 8b)}$$

$$\dot{R}^{v}_{eff} = s^{v}_{Li_2O_2} k_{eff}\left(c_{RM^+}\text{-}\frac{c_{RM}}{K^{eq}_{eff}} a_{Li^+}\right) \qquad \text{(eq. 9)}$$

On-line electrochemical mass spectrometry measurement

An in-house constructed two compartment cell, where the anode and cathode compartments are separated with a Li-conducting ceramic (Ohara) was used for the on-line electrochemical mass spectrometry (OEMS) measurements. The cathode compartment of the cell was continuously fluxed with Ar gas, controlled with a mass flow controller, which is then passed into a mass spectrometer to detect gaseous products. The cathodes were fabricated by mixing Li_2O_2, Ketjen black carbon and PTFE (4/4/2 weight ratio) to obtain a dry paste. The paste was pressed into pellets with a 7 mm diameter die set, to provide a mass loading of 12 mg/cm^2. The pellets were then pressed onto stainless steel mesh current collectors. All the above-mentioned fabrication procedures were conducted in an Ar-filled glovebox. Li metal pellets were used as anodes. 1 M LiTFSI in tetraglyme was used as the anolyte and 1 M LiTFSI in tetraglyme containing 10 mM of redox mediator (TEMPO, TMPD or DMPZ) was used as the catholyte.

The mass spectrometer was quantitatively calibrated using standards of known gas content. Quantification methodology involves estimating the fraction of gas in the sample by comparing the ionic flux detected from the sample gas to the calibration standard. Gas fraction is converted into moles per minutes by multiplying the flow rate and using the ideal gas law to convert from volume to moles.

Experimental determination of kinetics of superoxide oxidation

A saturated solution of KO_2 is made by stirring solid KO_2 in tetraglyme for an hour and filtering to yield a clear yellow solution. A known concentration of $DMPZ^+$ (prepared following the method described above) was added to the saturated KO_2 solution with rapid stirring while measuring UV-Vis in-situ (Oceanoptics DH-2000 with Deuterium-Halogen light source and Oceanoptics flame miniature spectrometer) to track the change in $DMPZ^+$ concentration as it oxidises KO_2. The rate of change in $DMPZ^+$ concentration is proportional to the rate of reaction. In order to study the effect of cation coordination on superoxide reactivity, this measurement was repeated with the addition of 18-crown-6-ether, which is known to bind strongly to K^+. All measurements were carried out in a nitrogen glovebox with < 1 ppm H_2O and O_2.

Stability of TEMPO·BF_4

Solid TEMPO·BF_4 is synthesized following a literature method.[28] This is dissolved in 0.1 M LiTFSI tetraglyme to make up 10 mM TEMPO·BF_4 solution. This solution is aged for varying lengths of time before adding to Li_2O_2 stored in a stoppered vial with a gas inlet and outlet through which argon flowed at a rate of 0.35 mL min^{-1} before passing to an on-line mass spectrometer to evaluate the triplet oxygen evolved.

Singlet oxygen quantification by HPLC

Synthesised Li_2O_2 (> 99%) and oxidised RM were added to a stoppered vial with a gas inlet and outlet through which argon flowed at a rate of 0.35 mL min^{-1} before passing to an on-line mass-spectrometer to evaluate the triplet oxygen evolved. No oxygen evolution was observed when mixing the solid reactants. The reaction was initiated by injection of tetraglyme (which dissolves the mediator) containing 30 mM 9,10-dimethylanthracene (DMA),[21] which reacts rapidly with $^1O_2$ to form 9,10-dimethylanthracene-endoperoxide (DMA-O_2) in solution. The reaction mixture was stirred using a magnetic stirrer bar. UV-Vis spectra of DMA and DMA-O_2 is shown in Fig. S12. Organic endoperoxides are known to convert back to $^1O_2$ and DMA when heated at 60 ^{0}C and above.[70,71] All DMA and DMA-O_2 were handled at room temperature with minimal exposure to light.

The amount of triplet oxygen ($^3O_2$) released was quantified from the mass spectrometry. Following the procedure developed by Freunberger et al., $^1O_2$ released was determined by quantification of DMA-O_2 by High-Performance-Liquid-Chromatography (HPLC) with a UV-vis detector (1200 series, Agilent Technologies), calibrated using DMA-O_2 solutions of known concentration.[21] Standard DMA-O_2 solutions were made by exposing DMA solution to singlet oxygen generated by 5,10,15,20-Tetraphenyl-21H,23H-porphine sensitizer (TPP, < 1% concentration of DMA) excited with a 660 nm light source for several hours while bubbling dried $^3O_2$ (N5.0 grade, BOC). As it is possible for $^1O_2$ to be quenched by other chemical and physical pathways rather than reaction with DMA, $^1O_2$ amount quantified using this method can only be taken as the minimum amount, as such it is only used to evaluate the trend in $^1O_2$ formation.

It is known that LiO_2 is thermodynamically unstable, so to quantify $^1O_2$ formation during LiO_2 disproportionation, so we follow well-established methods starting with KO_2 precursor.[72,73] 1.5 to 15 mg of KO_2 is weighed into a sealed and air-tight vial connected to an on-line mass spectrometer. 1.5 ml of 1 M LiTFSI with 0.1 M crown-6-ether and 30 mM DMA in tetraglyme is injected into the vial with rapid stirring. $^3O_2$ release is quantified with online mass spectrometry, while $^1O_2$ is captured by DMA which is quantified using HPLC. $^1O_2$ yield is calculated following $^1O_2$/ ($^1O_2$ + $^3O_2$). This is repeated three times with varying amounts of KO_2, to get an average $^1O_2$ yield and the associated standard error.

Singlet oxygen quantification by NMR

The evolution of $^1O_2$ during Li_2O_2 oxidation by RMs was studies with DMA and nuclear magnetic resonance (NMR) spectroscopy (υ_0 = 600.13 MHz, with a proton-optimised TCI HCN cryoprobe). For NMR samples, 60 mM DMA in tetraglyme was injected onto a vial containing an excess of in-house synthesised of Li_2O_2 and RM^+ (equivalent to 10 mM) with stirring throughout the reaction. $^3O_2$ evolution was monitored by on-line mass-spectrometry, and the solutions were filtered once O_2 evolution ceased. Following the literature,[18] DMA was used to detect $^1O_2$ through formation of $DMAO_2$. We note that $DMAO_2$ is known to form $DMA(OH)_2$ in the presence of protons, and this can be detected in the NMR as deshielded aromatic -CH resonances at 8.5 and 7.7 ppm, Fig. S10a and b). The -OH groups are observed as broadened density at 6.5 ppm, consistent with -OH groups neighbouring aromatic systems and a singlet at 1.0 ppm is observed for the methyl groups. The isolation of these aromatic resonances and lack of obstruction from the neighbouring DMA peaks and their ^{13}C satellites means they can be accurately integrated to determine the concentration of the $DMA(OH)_2$. The lower detection limit using this high-field NMR experiment with a ^{1}H-optimised cryoprobe and an 18-hour quantitative (T_1 = ~3 s, D_1 = 30 s, $^{\pi}/_2$ direct observe experiment) experiment is 2 µM. These experiments show only 0.10 % $^1O_2$ in the $TEMPO^+$ samples. In contrast, NMR analysis of low voltage RMs suggests

3.69 % and 12.5 % $^1O_2$ from Li_2O_2 oxidation by $TMPD^+$ and TTF^+, respectively. These values are tabulated in Table S1 for comparison with HPLC data. While the absolute values of singlet oxygen yield obtained from HPLC and NMR are not identical (noting that the latter detects both $DMAO_2$ and $DMA(OH)_2$, the trends agree in that low voltage RMs evolve more singlet oxygen than high voltage RMs from both methods, confirming that the trend shown in Fig. 4 is correct.

Data availability

Data supporting the main findings of this work are available within the Article and Supplementary Information. Source data are provided with this paper.

Code availability

The Comsol code for gas diffusion electrode electrochemical model simulations is available as a compressed file as Supplementary Code 1.

Methods-only references

59. Ergun, S., Elliott, C. F., Preet Kaur, A., Parkin, S. R. & Odom, S. A. Overcharge performance of 3,7-disubstituted N-ethylphenothiazine derivatives in lithium-ion batteries. *Chem. Commun.* **50**, 5339–5341 (2014).

60. Ma, Z. & Bobbitt, J. M. Organic Oxoammonium Salts. A New Convenient Method for the Oxidation of Alcohols to Aldehydes and Ketones. *J. Org. Chem.* 6110–6114 (1991).

61. Giffard, M. *et al.* Oxidation of TTF derivatives using (diacetoxyiodo)benzene: A general chemical route toward cation radicals, dications, and nonstoichiometric salts [18]. *J. Am. Chem. Soc.* **123**, 3852–3853 (2001).

62. Reiners, M. *et al.* Teaching Ferrocenium How to Relax: A Systematic Study on Spin–Lattice Relaxation Processes in tert-Butyl-Substituted Ferrocenium Derivatives. *Eur. J. Inorg. Chem.* **2017**, 388–400 (2017).

63. Michaelis, L. & Granick, S. The Polymerization of the Free Radicals of the Wurster Dye Type: The Dimeric Resonance Bond. *J. Am. Chem. Soc.* **65**, 1747–1755 (1943).

64. Dobrynina, T. A., Akhapkina, N. A. & Chuvaev, V. F. Synthesis and properties of lithium peroxide monoperoxyhydrate Li2O2·H2O2. *Bull. Acad. Sci. USSR Div. Chem. Sci.* **18**, 438–440 (1969).

65. Cornut, R. & Lefrou, C. A unified new analytical approximation for negative feedback currents with a microdisk SECM tip. *J. Electroanal. Chem.* **608**, 59–66 (2007).

66. Zhao, Y. H., Abraham, M. H. & Zissimos, A. M. Fast calculation of van der Waals volume as a sum of atomic and bond contributions and its application to drug compounds. *J. Org. Chem.* **68**, 7368–7373 (2003).

67. Nohra, B. *et al.* Polyoxometalate-based metal organic frameworks (POMOFs): Structural trends, energetics, and high electrocatalytic efficiency for hydrogen evolution reaction. *J. Am. Chem. Soc.* **133**, 13363–13374 (2011).

68. Wang, Y. *et al.* A Solvent-Controlled Oxidation Mechanism of Li 2 O 2 in Lithium-Oxygen Batteries. *Joule* **2**, 2364–2380 (2018).

69. Gao, X., Chen, Y., Johnson, L. & Bruce, P. G. Promoting solution phase discharge in Li–O2 batteries containing weakly solvating electrolyte solutions. *Nat. Mater.* **15**, 882–888 (2016).

70. Turro, N. J., Chow, M. F. & Rigaudy, J. Mechanism of Thermolysis of Endoperoxides of Aromatic Compounds. Activation Parameters, Magnetic Field, and Magnetic Isotope Effects. *J. Am. Chem. Soc.* **103**, 7218–7224 (1981).

71. Adam, W., Kazakov, D. V. & Kazakov, V. P. Singlet-oxygen chemiluminescence in peroxide reactions. *Chem. Rev.* **105**, 3371–3387 (2005).

72. Black, R. *et al.* Screening for superoxide reactivity in Li-O 2 batteries: Effect on Li 2O 2/LiOH crystallization. *J. Am. Chem. Soc.* **134**, 2902–2905 (2012).

73. Peng, Z. *et al.* Oxygen reactions in a non-aqueous Li+ electrolyte. *Angew. Chemie - Int. Ed.* **50**, 6351–6355 (2011).

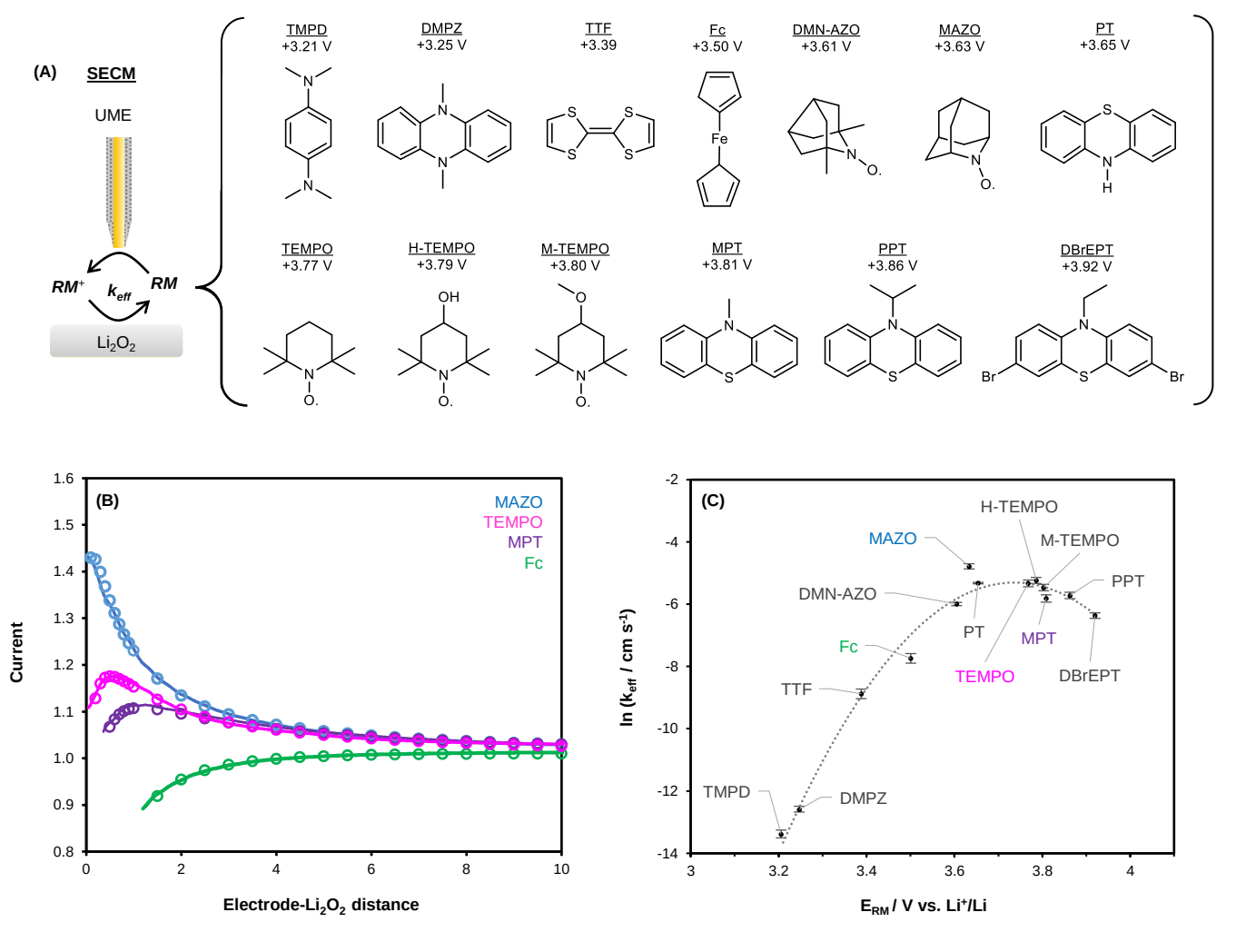
(A)
SECM
UME
RM+
keff
RM
Li2O2
TMPD
+3.21 V
DMPZ
+3.25 V
TTF
+3.39
Fc
+3.50 V
DMN-AZO
+3.61 V
MAZO
+3.63 V
PT
+3.65 V
TEMPO
+3.77 V
H-TEMPO
+3.79 V
M-TEMPO
+3.80 V
MPT
+3.81 V
PPT
+3.86 V
DBrEPT
+3.92 V
(B)
MAZO
TEMPO
MPT
Fc
Current
Electrode-Li2O2 distance
(C)
H-TEMPO
MAZO
M-TEMPO
PPT
DMN-AZO
PT
MPT
Fc
TEMPO
DBrEPT
TTF
TMPD
DMPZ
ln (keff / cm s-1)
ERM / V vs. Li+/Li

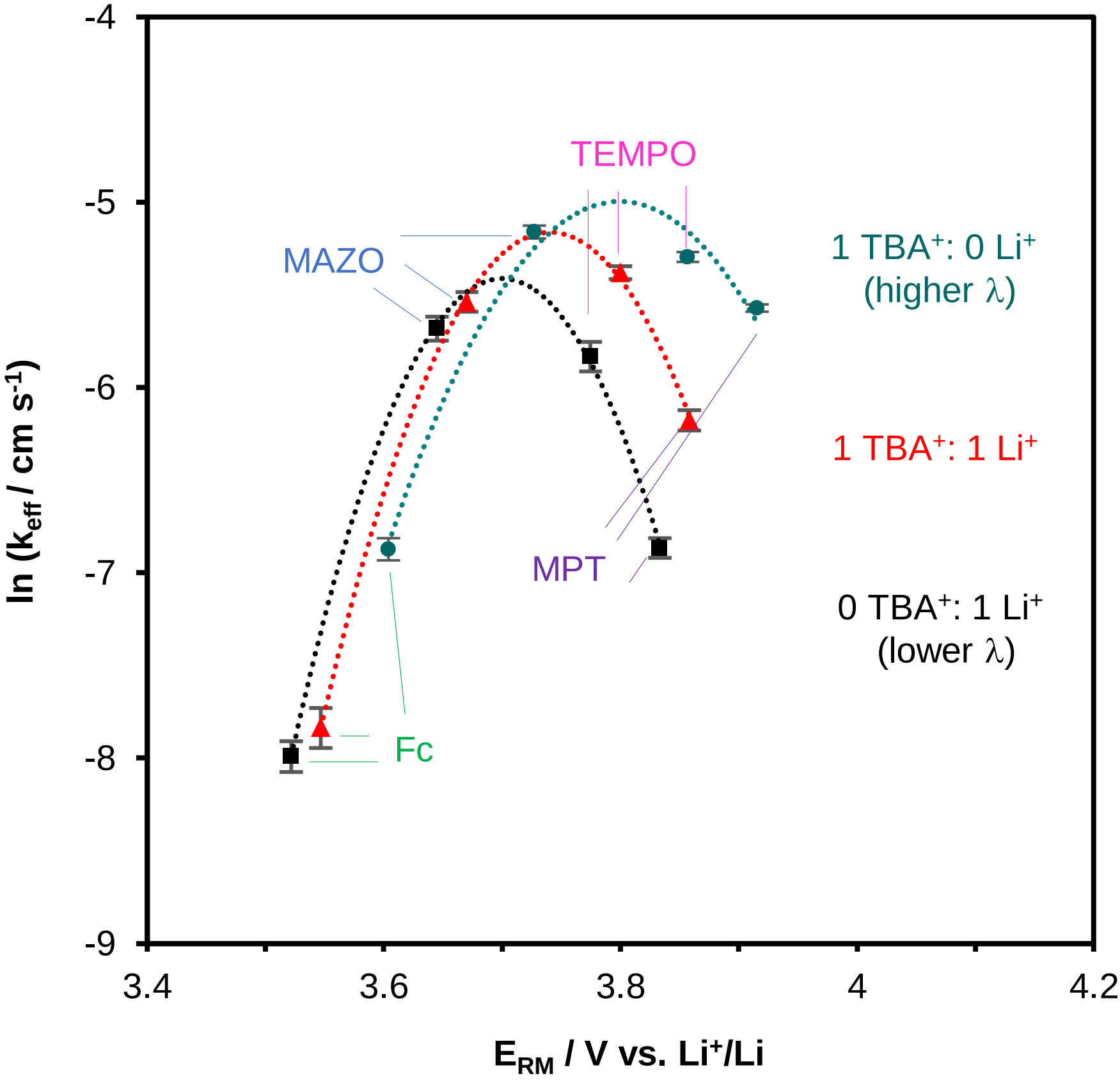
-4
-5
-6
-7
-8
-9
3.4
3.6
3.8
4
4.2
ln (k_eff / cm s^-1)
E_RM / V vs. Li+/Li
TEMPO
MAZO
MPT
Fc
1 TBA+: 0 Li+
(higher λ)
1 TBA+: 1 Li+
0 TBA+: 1 Li+
(lower λ)

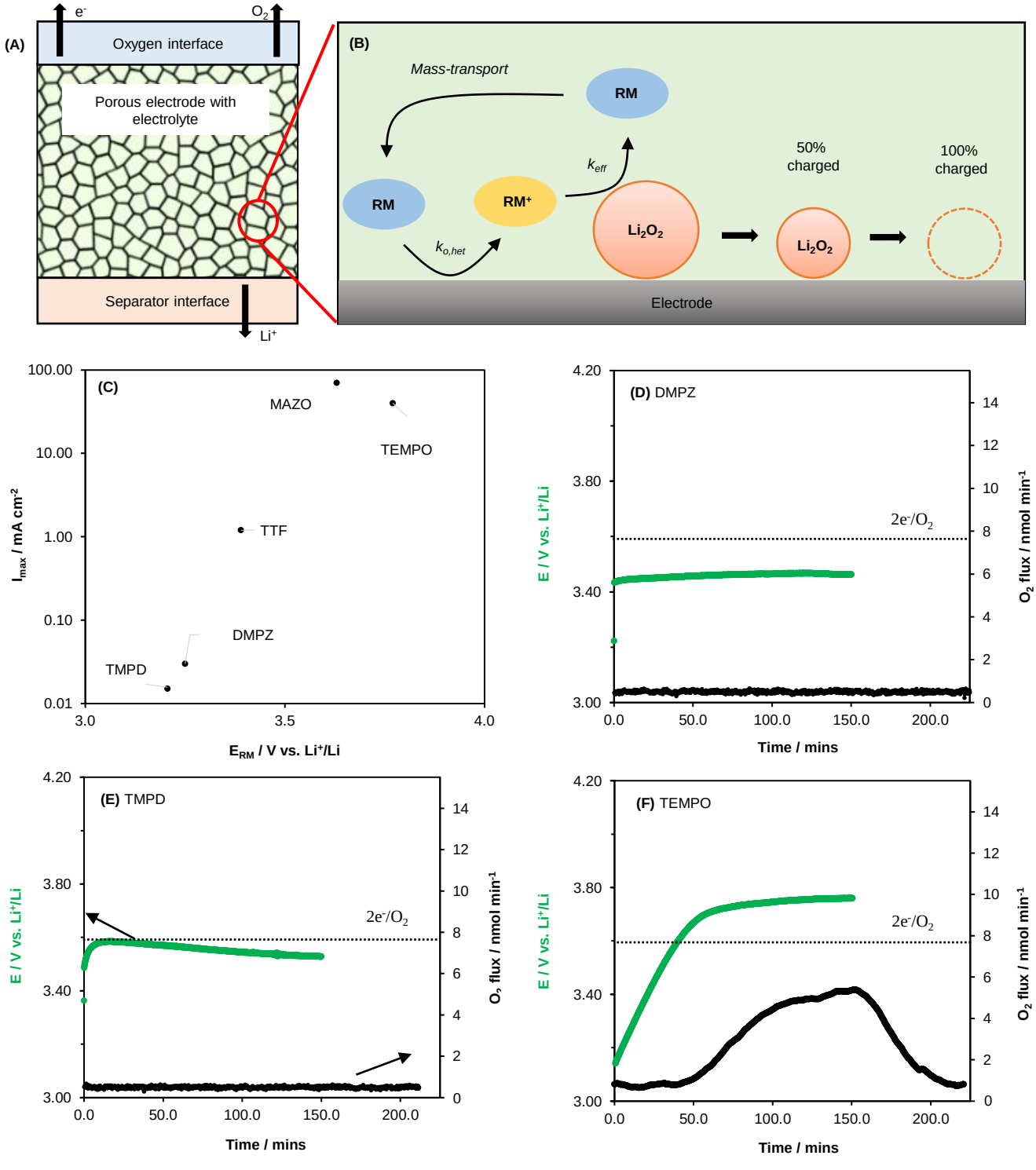
(A)
e-
O2
Oxygen interface
Porous electrode with electrolyte
Separator interface
Li+
(B)
Mass-transport
RM
keff
RM
RM+
ko,het
Li2O2
50% charged
Li2O2
100% charged
Electrode
(C)
MAZO
TEMPO
TTF
DMPZ
TMPD
Imax / mA cm-2
ERM / V vs. Li+/Li
(D) DMPZ
2e-/O2
E / V vs. Li+/Li
O2 flux / nmol min-1
Time / mins
(E) TMPD
2e-/O2
E / V vs. Li+/Li
O2 flux / nmol min-1
Time / mins
(F) TEMPO
2e-/O2
E / V vs. Li+/Li
O2 flux / nmol min-1
Time / mins

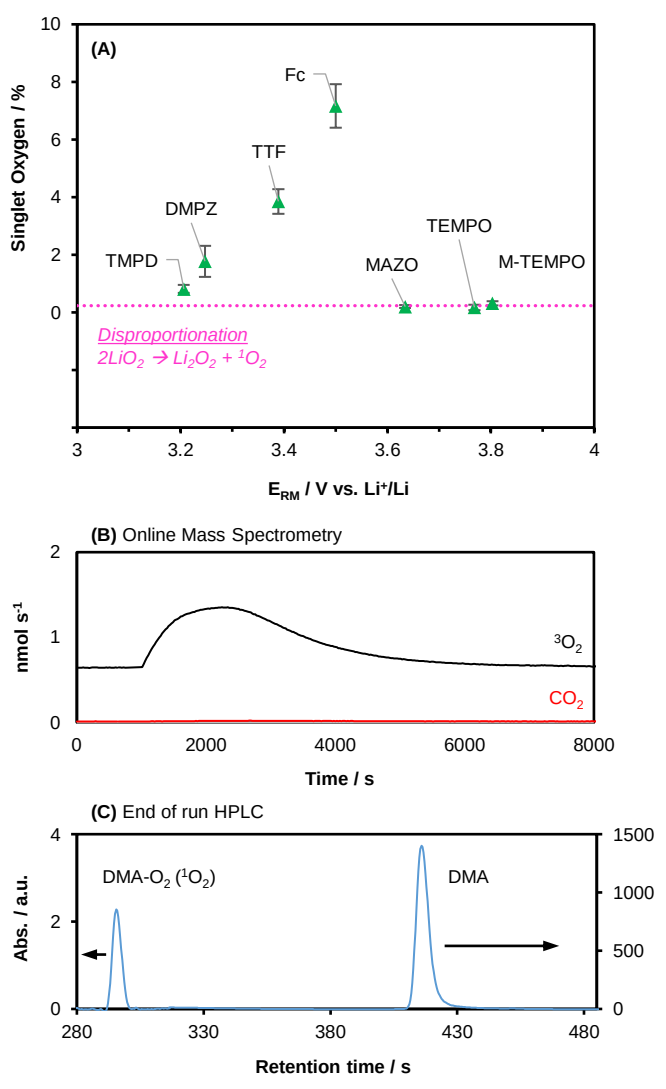
(A)
Singlet Oxygen / %
Fc
TTF
DMPZ
TMPD
TEMPO
MAZO
M-TEMPO
Disproportionation
2LiO2 → Li2O2 + 1O2
E_RM / V vs. Li+/Li
(B) Online Mass Spectrometry
nmol s-1
3O2
CO2
Time / s
(C) End of run HPLC
Abs. / a.u.
DMA-O2 (1O2)
DMA
Retention time / s

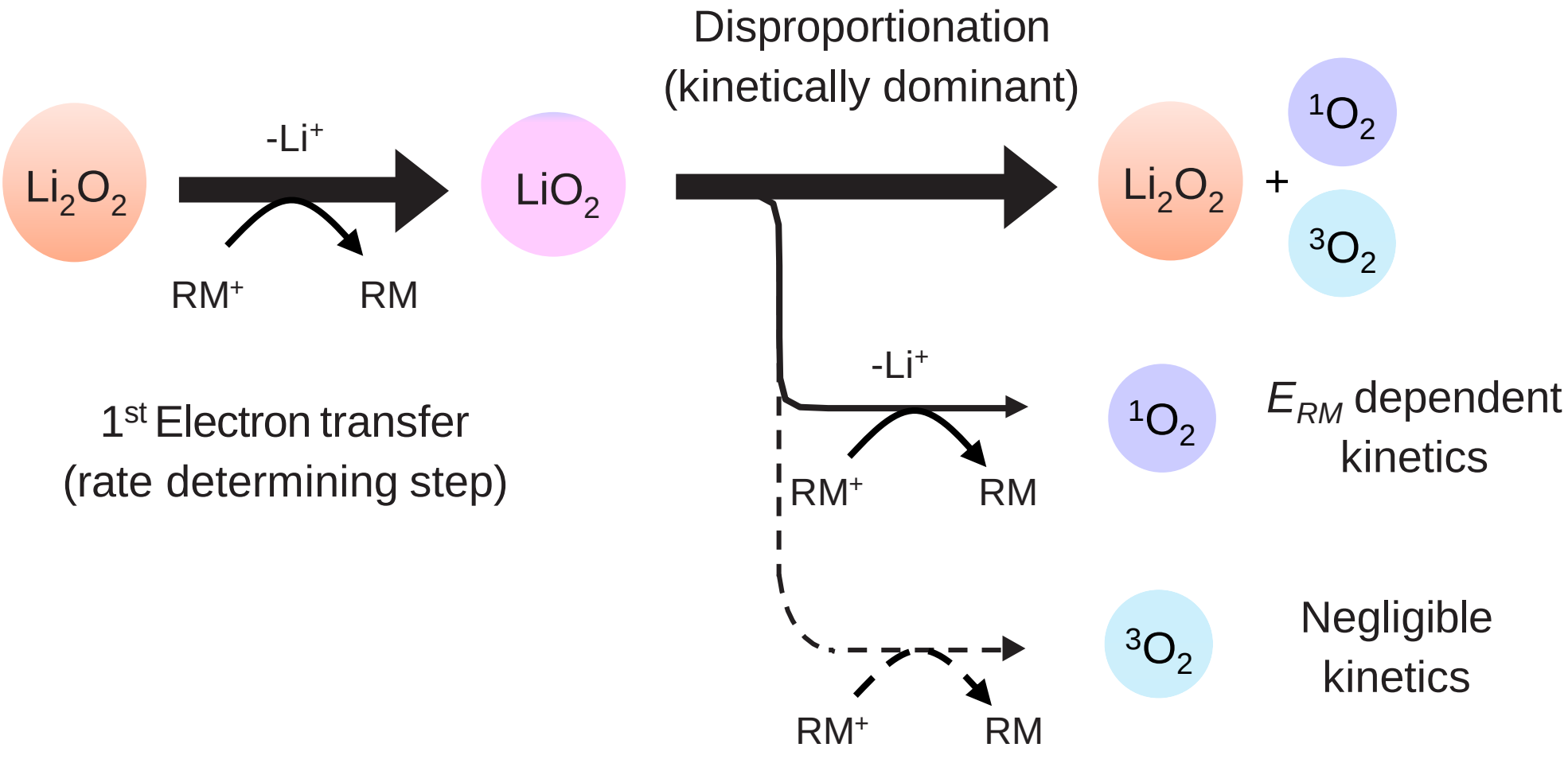
Disproportionation
(kinetically dominant)
Li_2O_2
-Li^+
LiO_2
RM^+
RM
1st Electron transfer
(rate determining step)
Li_2O_2
+
$^1O_2$
$^3O_2$
-Li^+
RM^+
RM
$^1O_2$
E_{RM} dependent
kinetics
RM^+
RM
$^3O_2$
Negligible
kinetics